Sustainable Energy & Fuels

ROYAL SOCIETY OF CHEMISTRY

PAPER

View Article Online
View Journal | View Issue

Cite this: *Sustainable Energy Fuels*, 2025, **9**, 5673

Enhancing pH-gradient microscale bipolar interfaces (PMBI) enabled direct methanol hydrogen peroxide fuel cell (DMHPFC) performance under varying operating conditions

Kritika Sharma,[a] Shrihari Sankarasubramanian,[bc] Zhongyang Wang[d] and Vijay Ramani *[a]

This study introduces a direct methanol hydrogen peroxide fuel cell (DMHPFC) using a pH-gradient-enabled microscale bipolar interface (PMBI) to address limitations in direct methanol fuel cells (DMFCs). Unlike conventional fuel cells that use oxygen, the DMHPFC utilizes H_2O_2, enhancing reactant availability and reaction kinetics. The PMBI maintains separate pH environments at the anode and cathode. The PMBI-DMHPFC combines an alkaline anode for methanol oxidation and an acidic cathode for hydrogen peroxide reduction, achieving a theoretical open-circuit voltage (OCV) of 1.72 V (compared to a theoretical OCV of 1.25 V for DMFCs) and a volumetric energy density of 9.2 kWh l^{-1} using aqueous methanol (39% vol) and hydrogen peroxide (41% vol). This energy density quadruples that of compressed hydrogen (2.1 kWh l^{-1} at 69 MPa). This study identifies optimal operating conditions: 5 M methanol with 3 M KOH as anolyte, 5 M hydrogen peroxide with 1.5 M sulfuric acid as catholyte, Nafion 115 (127 μm) as membrane, and flow rate of 2.5 ml min^{-1} cm^{-2} – that maximize the power output and minimize activation-, ohmic- and mass transfer losses in DMHPFCs. Performance evaluation reveals a measured OCV of 1.69 V. While the PMBI-DMHPFC surpasses DMFC performance, its high OCV and energy density are not fully translated into high power density due to significantly higher activation and mass transport losses compared to H_2–O_2 fuel cells, which typically achieve peak power densities above 1000 mW cm^{-2}. The DMHPFC achieves a peak power density of 630 mW cm^{-2} at the unusually high voltage of 0.8 V, reflecting the unique PMBI design and optimized operating conditions that reduce losses. This steeper voltage drop is attributed to sluggish reaction kinetics, membrane crossover and mass transport limitations. It highlights the potential for improved performance through advanced electrocatalysts, optimized membrane materials and flow design from this promising baseline.

Received 30th July 2025
Accepted 26th August 2025

DOI: 10.1039/d5se01042j

rsc.li/sustainable-energy

1 Introduction

Selecting an appropriate fuel and oxidant is fundamental to ensuring fuel cells' technical and economic viability. Hydrogen-fed polymer electrolyte membrane fuel cells (H_2-PEMFCs), which use hydrogen as fuel and oxygen as the oxidant, are a well-established and widely studied technology.[1] However, their dependence on hydrogen is constrained by the lack of adequate infrastructure for its storage and distribution in both liquid and gaseous forms.[2,3] As an alternative, direct liquid fuel cells (DLFCs) have gained attention due to their ease of handling liquid fuels and compatibility with existing infrastructure.[4] Among DLFCs,[5–7] direct methanol fuel cells (DMFCs) are particularly notable. Methanol's high energy density (4.3 kWh l^{-1}), good electrochemical activity, widespread availability with annual global production exceeding 79 million metric tons (projected to approach 100 million metric tons by 2030),[8] biodegradability, and low cost—currently around $350–$450 per metric ton,[9] make it an attractive fuel option.[10] It can also be directly fed into the anode, without requiring a reforming process, simplifying the system.[11] While toxic, its risks are manageable in commercial applications.[12] However, unlike H_2-PEMFCs, where kinetic losses are primarily at the cathode, DMFCs experience low power density due to sluggish kinetics at both electrodes (methanol oxidation reaction (MOR)[13] and oxygen reduction reaction (ORR)[14]).

[a]*Department of Energy, Environmental and Chemical Engineering, Washington University in St. Louis, One Brookings Dr., St. Louis, MO 63130, USA. E-mail: ramani@wustl.edu*

[b]*Department of Biomedical Engineering and Chemical Engineering, The University of Texas at San Antonio, San Antonio, TX 78249, USA*

[c]*Department of Mechanical, Aerospace and Industrial Engineering, The University of Texas at San Antonio, San Antonio, TX 78249, USA*

[d]*Department of Chemical and Biological Engineering, University of Alabama, Tuscaloosa, AL 35487, USA*

To address the issue of low power density and overcome the limitations of oxygen as an oxidant, this study explores an innovative configuration of fuel and oxidant: the direct methanol hydrogen peroxide fuel cell (DMHPFC). H_2O_2 presents several advantages over O_2 as an oxidant.[15–17] First, as a liquid, H_2O_2 offers enhanced reactant availability at catalyst sites. Gaseous reactants like oxygen require effective diffusion through gas diffusion layers and efficient dissolution at the catalyst surface, processes that limit performance. Second, H_2O_2 exhibits improved reaction kinetics, which can be attributed to its lower O–O bond enthalpy (144 kJ mol^{-1}) compared to O_2 (498 kJ mol^{-1}).[18] This lower bond energy facilitates easier bond breaking and faster reaction rates during the hydrogen peroxide reduction reaction (HPRR). This is particularly important at the cathode, where ORR is often a major bottleneck. Third, using H_2O_2 enables fuel cell operation in oxygen-free environments, such as underwater or in space. Both MOR and HPRR are pH dependent reactions. The MOR kinetics in alkaline media exhibit faster reaction rates than in acidic media, with activity decreasing in the order of NaOH > Na_2CO_3 > $NaHCO_3$.[19] In contrast, acidic media is preferred for H_2O_2 due to reduced ionization-induced decomposition.[20] The theoretical potentials for the MOR and HPRR depend on the pH of the medium and are referenced *versus* the Standard Hydrogen Electrode (SHE) with explicit pH values. Specifically, the theoretical potential for MOR is −0.78 V *vs.* SHE at pH 14 (alkaline media) and −0.02 V *vs.* SHE at pH 0 (acidic media).[21] In contrast, the theoretical potential for HPRR is 1.77 V *vs.* SHE at pH 0 (acidic media) and 0.87 V *vs.* SHE at pH 14 (alkaline media).[21] Combining an alkaline anode for MOR with an acidic cathode for HPRR offers a promising configuration for achieving the highest possible theoretical open circuit voltage (OCV). As shown in Fig. 1a, this configuration yields an OCV of 1.72 V after accounting for the bipolar junction potential from water dissociation (−0.83 V).[22,23] The bipolar junction potential arises from the interfacial ion transfer resistance between the acidic

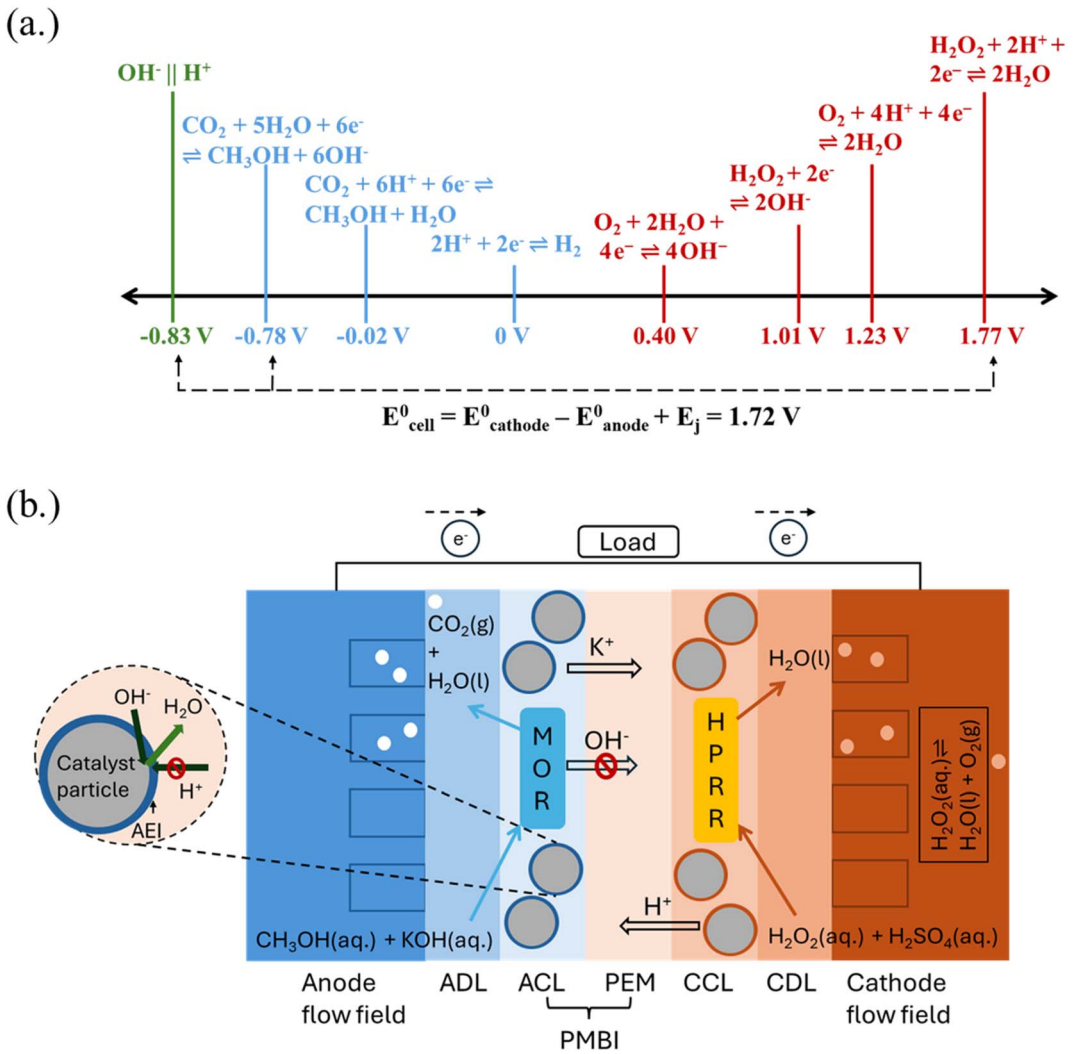

Fig. 1 (a) Half-cell reactions at the anode (blue) and cathode (red). The reactions are presented in balanced reduction form with standard reduction potentials (E^0) shown for half-cell redox reactions only. The junction potential at the PMBI interface (green) is explicitly labeled as the junction potential. (b) Working principle of the PMBI-DMHPFC.

and alkaline environments. The key to this configuration is maintaining distinct pH environments, which can be achieved here using a pH-gradient-enabled microscale bipolar interface (PMBI).[24] Previously explored in direct borohydride hydrogen peroxide fuel cells (DBHPFCs),[24–26] the PMBI function is to maintain a localized alkaline environment at the anode even as bulk conditions near the anode remain non-alkaline due to the acidity of the cathode. This approach ensures sustained MOR activity and mitigates performance degradation caused by pH imbalance.

In addition to high theoretical OCV, a DMHPFC's energy density is higher than H_2-PEMFCs. Current state-of-the-art fuel cells typically store H_2 gas at 69 MPa. The volume-specific energy density for H_2 gas stored at 69 MPa is 2.1 kWh l^{-1}.[27] In contrast, aqueous methanol (39% by volume) and aqueous hydrogen peroxide (41% by volume) correspond to a volume-specific energy density of approximately 9.2 kWh l^{-1},[27] comparable to gasoline, which also contains about 9.2 kWh l^{-1} of available bond energy. This makes the DMHPFC's energy density per unit volume nearly four times greater than that of H_2-PEMFC, offering a compelling advantage for applications requiring compact energy storage. However, despite its high energy density, the DMHPFC is currently constrained by its low power density. While H_2-PEMFCs achieve peak power density (PPD) of approximately 1000 mW cm^{-2},[28] prior DMHPFC reaches only about 125 mW cm^{-2} (ref. 29)—nearly 8 times lower. This disparity necessitates larger, heavier stacks to match power output, limiting their viability in weight- and size-sensitive applications like portable electronics or transportation systems.

This work develops a PMBI-DMHPFC, achieving an OCV of 1.69 V and PPD of approximately 630 mW cm^{-2} at 0.8 V, exceeding the OCVs and PPDs of previous DMFC designs. Furthermore, the effects of operating conditions, including anolyte and catholyte concentrations, membrane thickness, and flow rate on the DMHPFC performance, are systematically explored to reveal the underlying performance characteristics of the PMBI-DMHPFC system. This exploration aims to identify optimal operating conditions to maximize efficiency and guide future performance-enhancing strategies.

2 Working principle

The PMBI-DMHPFC, illustrated in Fig. 1b, consists of an alkaline anode compartment and an acidic cathode compartment separated by a PMBI. The anode comprises a catalyst layer (ACL), where the MOR occurs, a diffusion layer (ADL) for efficient methanol transport, and a flow field (AFF) to ensure uniform methanol distribution. Similarly, the cathode comprises a catalyst layer (CCL) for the HPRR, a diffusion layer (CDL), and a flow field (CFF). PMBI comprises the proton exchange membrane (PEM) intimately interfaced with a thin layer of anion exchange ionomer (AEI) binder at the ACL, which plays a critical role in maintaining localized alkaline conditions at the anode while preventing pH crossover.[24] During operation, an aqueous MeOH and hydroxide (OH^-) solution is supplied to the anode, flowing through the AFF and diffusing through the ADL to reach the ACL. At the ACL, methanol undergoes oxidation in the presence of OH^- according to the reaction:

$$CH_3OH + 6OH^- \rightarrow 6e^- + CO_2 + 5H_2O;\quad E_{0,\ anode} = -0.78\ V\ vs.\ SHE \quad (1)$$

The generated electrons are then transported through an external circuit to the cathode, providing electrical power to the load. The resulting carbon dioxide (CO_2) and water enter the AFF before exiting the system. Simultaneously, a solution containing H_2O_2 and protons (H^+) is supplied to the cathode, flowing through the CFF, and diffusing through the CDL to reach the CCL. At the CCL, H_2O_2 is reduced according to the reaction:

$$3H_2O_2 + 6H^+ + 6e^- \rightarrow 6H_2O;\ E_{0,\ cathode} = 1.77\ V\ vs.\ SHE \quad (2)$$

At the PMBI, water dissociation occurs, generating H^+ ions, which diffuse toward the cathode and OH^- ions, which diffuse toward the anode under the influence of the electric field. This mechanism ensures the maintenance of distinct pH environments at each electrode.[22] This process is driven by the electrochemical potential gradient across the membrane and occurs at the PMBI interface rather than the electrodes. This process prevents pH crossover while allowing efficient ion transport.

$$H^+ + OH^- \rightarrow H_2O;\ E_j = -0.83\ V\ vs.\ SHE \quad (3)$$

The overall cell reaction is:

$$CH_3OH + 3H_2O_2 + 6H^+ + 6OH^- \rightarrow CO_2 + 11H_2O;\ E_{0,cell} = 1.72\ V \quad (4)$$

As shown in Fig. 1, the theoretical OCV for this PMBI-DMHPFC is calculated as $E_{0,\ cell} = E_{0,\ cathode} - E_{0,\ anode} + E_j = 1.72$ V.

The overall cell reaction (eqn (4)) demonstrates the theoretical potential for high energy conversion in the PMBI-DMHPFC. However, achieving this potential in practice requires overcoming substantial overpotential barriers at both electrodes. At anode, the sluggish kinetics of MOR can be partially mitigated by using high loadings of precious metal catalysts, particularly platinum (Pt), albeit at a significant cost increase.[30] During MOR, carbon monoxide (CO) forms as a reaction intermediate and strongly adsorbs on the Pt catalyst surface,[31] blocking active sites and impeding further reaction. Mitigating CO poisoning requires a higher anodic overpotential to oxidize adsorbed CO into CO_2, thereby freeing active sites for MOR.[32] To mitigate CO poisoning, binary alloys have been employed, with Pt–Ru outperforming others due to its superior CO tolerance and catalytic activity.[33] The Ru component provides oxygenated species (OH) at lower potentials,[34] which react with CO adsorbed on adjacent Pt sites, oxidizing it to CO_2. This bifunctional mechanism,[34] coupled with Ru's modification of Pt's electronic structure,[35,36] weakens the Pt–CO bond[37] and enhances CO removal. While other binary alloys (*e.g.*, Pt–Ni, Pt–Mo, Pt–Au, Pt–TiO_2) show

promise in specific aspects, they generally underperform compared to Pt–Ru in overall performance and CO tolerance. For example, Pt–Ni[38] and Pt–Mo[39] show good activity but lower CO tolerance, Pt–Au[40] has good stability but lower MOR activity, and Pt–TiO_2 (ref. 41) offers improved CO tolerance but lower overall catalytic activity. Consequently, Pt–Ru was selected as the MOR catalyst for this work due to its superior resistance to poisoning and overall catalytic efficiency. In addition to CO poisoning challenges at the anode, CO_2 bubbles produced during MOR (eqn (1)) can block active catalyst sites and hinder reactant transport to these sites, causing mass transport limitations. Another challenge at the anode is the crossover of H_2O_2 from the cathode, which leads to mixed potentials.

Moving to the cathode, the HPRR presents its own complexities. A Pt catalyst is used at the cathode for its high catalytic activity for HPRR. In addition to HPRR, side reactions involving hydrogen peroxide decomposition (eqn (5)) and complete and incomplete ORR (eqn (6) and (7), $E^0 = 1.23$ V and 0.69 V *vs.* RHE, respectively[21]) can occur. The potentials associated with these ORR pathways are lower than that of HPRR (eqn (2)), resulting in mixed potentials at the cathode. The decomposition of H_2O_2 is a first-order reaction, consequently, higher H_2O_2 concentrations lead to increased decomposition rates, resulting in more significant oxygen generation.[42] Furthermore, the O_2 bubbles produced by eqn (5) can occupy Pt catalyst sites, leading to mass transport limitations. Analogous to H_2O_2 crossover to the anode, MeOH crosses through the PEM to the cathode. The crossover methanol creates a competing reaction at the cathode.[43] The crossover methanol can be incompletely oxidized to CO, $CHOH^-$, and CHO^-, deactivating the cathode catalyst.[44]

$$2H_2O_2 \rightarrow O_2 + 2H_2O \quad (5)$$

$$O_2 + 4e^- + 4H^+ \rightarrow 2H_2O;\ E^0 = 1.23\ \textit{vs.}\ \text{RHE} \quad (6)$$

$$O_2 + 2e^- + 2H^+ \rightarrow 2H_2O_2;\ E^0 = 0.69\ \textit{vs.}\ \text{RHE} \quad (7)$$

In summary, the PMBI-DMHPFC offers a promising configuration for efficient energy conversion, but its performance is influenced by various overpotentials at both the anode and cathode, necessitating further optimization.

3 Materials and methods

3.1 Materials

Methanol (99.9%), KOH (90%), hydrogen peroxide (30%), sulfuric acid (99.999%), chlorobenzene (99.5%), tin(IV) chloride (99.995%), chlorotrimethylsilane (99%), chloroform (99.5%), paraformaldehyde (99.5%), silver nitrate (0.1 N), potassium thiocyanate (0.1 N), sodium nitrate (99%), chloroform-d (99.96%), 1-methyl-2-pyrrolidinone (NMP) (99.7%), trimethylamine solution (TMA) (31–35% weight percent in ethanol), were purchased from Sigma Aldrich. SEBS (55 : 45 molar ratio of styrene to rubber, styrene–ethylene–butadiene–styrene) was sourced from Kraton Performance Polymers Inc.

3.2 Membrane electrode assembly

A carbon-supported Pt–Ru/C catalyst (1 : 1 weight ratio from Tanaka K. K) was used at the anode (MOR electrode). A suspension of 0.4 g Pt/Ru catalyst in a solution of 0.17 g CMSEBS55 (chloromethylated SEBS-55, degree of functionality: 0.27) in 9.75 ml of chlorobenzene was sonicated for 7 min. The CMSEBS-55 was synthesized using the procedure mentioned in prior work.[45] The resultant ink was sprayed on a porous nickel foam electrode (1.6 mm thickness from MTI Corporation) with an airbrush (Badger model 150). The electrode was immersed in a mixture of NMP (30 ml) and TMA solution (3 ml) at 30 °C for two days to functionalize the CMSEBS55 and yield the AEI (SEBS55-TMA). A carbon-supported Pt catalyst (46 weight% Pt/C from Tanaka K. K.) was used at the cathode (HPRR catalyst). A suspension of 0.4 g Pt/C catalyst in a 3.42 g Nafion® perfluorinated resin solution in 6 ml of isopropanol/water mixture (1 : 1 weight ratio) was sonicated for 7 min. The resultant ink was sprayed on porous carbon paper (GDL 24AA diffusion media from Ion Power) with an airbrush (Badger model 150). The nominal catalyst loadings at the anode and the cathode for the 5 cm^2 active area cell were 3 $mg_{catalyst}$ cm^{-2}. Nafion® membranes with different thicknesses were used as the membrane separator.

3.3 DMHPFC performance tests

DMHPFCs with the PMBI configuration were tested with a 5 cm^2 active cell area. The fuel cell performance was evaluated at 80 °C in a corrosion-resistant single-cell device (Fuel Cell Technologies, Inc.). Before fuel cell testing, the anode was immersed in 1 M KOH, the cathode was immersed in 1 M H_2SO_4, and the membrane was immersed in H_2O for 4 h at room temperature. The pinch (compression) used during the fuel cell hardware assembly for all fuel cell experiments was three mils on each side, and the torque used to assemble the cell was 25 lbs-in at each bolt. For the DMHPFC tests, the fuel used was 1–7 M MeOH in 2–7 M KOH, and the oxidant used was 1–7 M H_2O_2 in 0.5 to 2 M H_2SO_4. The membranes used were NHP (20 μm), N212 (51 μm), N115 (127 μm) and N117 (183 μm). The flow rates for both anode and cathode were varied from 1 ml min^{-1} cm^{-2} to 5 ml min^{-1} cm^{-2} using a masterflex peristaltic pump. Polarization curves were acquired using a Solatron analytical potentiostat (1470) by scanning the cell voltage from OCV to 0.05 V with a 0.1 V step voltage. The system was held at each cell voltage for 60 s. The constant current discharge curve was also acquired using a Solatron analytical potentiostat (1470), with the data acquisition rate set as 1 sample per minute.

4 Results and discussions

4.1 Performance of PMBI-DMHPFC

The performance of the PMBI-DMHPFC and a high-power density H_2-PEMFC[28] were comparatively analyzed *via* polarization and power density curves, as presented in Fig. 2a. As the figure illustrates, the PMBI-DMHPFC exhibited an impressive OCV of 1.69 V, surpassing that of H_2-PEMFCs by a factor of 1.8. This enhanced OCV is attributed to the unique

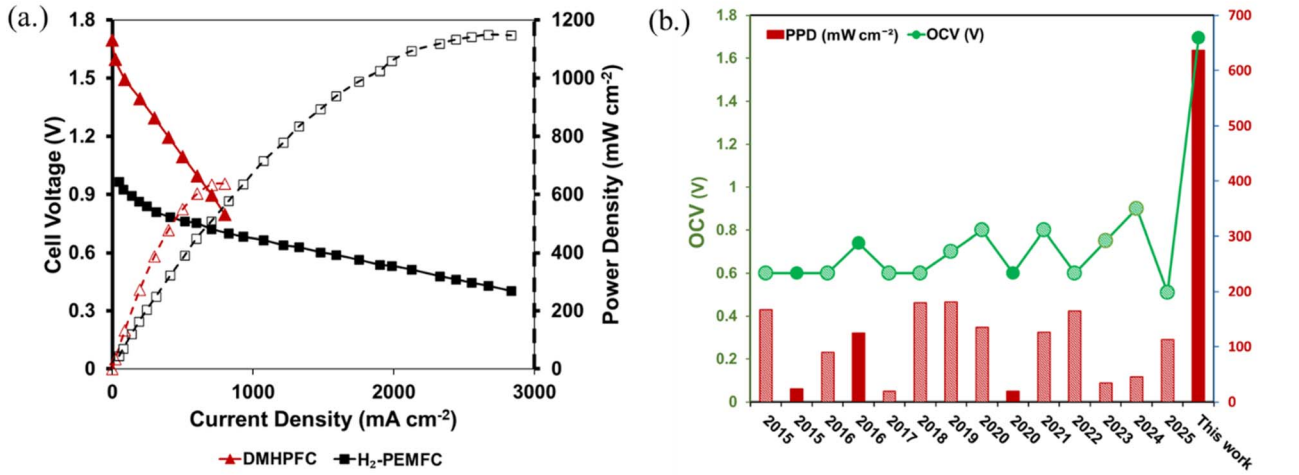

Fig. 2 (a) Polarization and power density curve of PMBI-DMHPFC and a high-power density H_2-PEMFCs. (b) Historical trend in DMFCs with oxidant as O_2 (shaded fill) and H_2O_2 (solid fill). The data is shown in Table S4.

thermodynamics of an alkaline anode medium and an acidic cathode medium. It should be noted that the observed high cell voltage is not attributable to a simple concentration cell mechanism. For a cell with only a pH gradient and hydrogen evolution/oxidation reactions occurring at the electrodes (a concentration cell), the maximum thermodynamic voltage is $\Delta E = 0.059\ \text{V} \times \Delta\text{pH}$, which is ~0.83 V for pH 0 to pH 14. In contrast, our system achieves an OCV of 1.69 V—well above this value—because the cell utilizes distinct redox couples: methanol oxidation at the alkaline anode ($E_{0,\text{anode}} = -0.78$ V *vs.* SHE at pH 14) and hydrogen peroxide reduction at the acidic cathode ($E_{0,\text{cathode}} = +1.77$ V *vs.* SHE at pH 0). These reactions are individually favorable and, when coupled, enable a high cell voltage with concomitant energy conversion, demonstrating that the cell is fundamentally a fuel cell, not a concentration cell. However, it is noteworthy that the measured OCV falls short of the theoretical value, which can be attributed to H_2O_2 decomposition, and MeOH and H_2O_2 crossover. The PMBI-DMHPFC's polarization curve demonstrated a steeper voltage drop than H_2-PEMFC, indicating greater polarization losses. The power density curves revealed a substantial difference in peak performance (Fig. 2a). The H_2-PEMFC achieved a PPD exceeding 1000 mW cm^{-2}, while the PMBI-DMHPFC reached a significantly lower PPD of approximately 600 mW cm^{-2}, approximately 1.6 times lower. This discrepancy can be explained by several factors inherent to the PMBI-DMHPFC system. Firstly, the electrochemical reactions in PMBI-DMHPFCs, specifically the MOR at the anode, is generally sluggish and more complex than hydrogen oxidation, leading to higher activation losses. In addition, the HPRR involves complex pathways at the cathode and is further complicated by the potential for H_2O_2 decomposition. Secondly, fuel and oxidant crossover reduces overall efficiency. Thirdly, mass transport limitations are exacerbated by CO_2 and O_2 bubbles forming during the electrochemical reactions. While these factors present challenges, advancements in DMFC technology have led to improved performance over time. Fig. 2b provides historical context by showing the OCV and PPD trend in DMFCs using oxygen O_2 and H_2O_2 as oxidants. The shaded bars represent DMFCs using O_2, while the solid bars represent using H_2O_2. The "This work" data point in Fig. 2b indicates that after optimizing the operating conditions, the PMBI-DMHPFC achieves a significantly higher OCV and PPD than earlier DMFCs. In addition to OCV and PPD, the energy efficiency of PMBI-DMHPFC is higher than that of DMFC (Table S2). The energy consumption of the PMBI-DMHPFC is higher than that of DMFCs (Table S2) due to the non-recirculation of fuel and oxidant solutions, leading to the loss of unused reactants. Introducing a recirculation system would significantly reduce energy consumption, balancing the superior power density and improving the fuel cell's competitiveness despite the additional energy demands of H_2O_2. However, Fig. 2a highlights room to improve PMBI-DMHPFC performance compared to the H_2-PEMFC. These results suggest that while the PMBI-DMHPFC offers a thermodynamic advantage reflected in its high OCV and thermodynamic efficiency (Section S2: thermodynamic efficiency of DMHPFC is ~91% whereas H_2-PEMFC can reach maximum thermodynamic efficiency of ~83%), further optimization of MOR and HPRR electrocatalysts, membrane materials to minimize fuel crossover, and cell architectures to improve mass transport are critical to enhance its performance and overall efficiency.

4.2 Effect of anolyte concentration

The concentration of MeOH in the fuel feed is a critical parameter influencing PMBI-DMHPFC performance, balancing fuel supply to the anode with the risks of MeOH crossover and mass transport limitations. To investigate this trade-off, the PMBI-DMHPFC was evaluated with varying MeOH concentrations (1 M to 7 M) while maintaining a fixed KOH concentration of 5 M (Fig. 3a). As shown in Fig. 3a, increasing the MeOH concentration from 1 M to 5 M elevates the MeOH content within the ACL, thereby enhancing MOR kinetics and reducing activation losses. This is evidenced by a slight increase in the

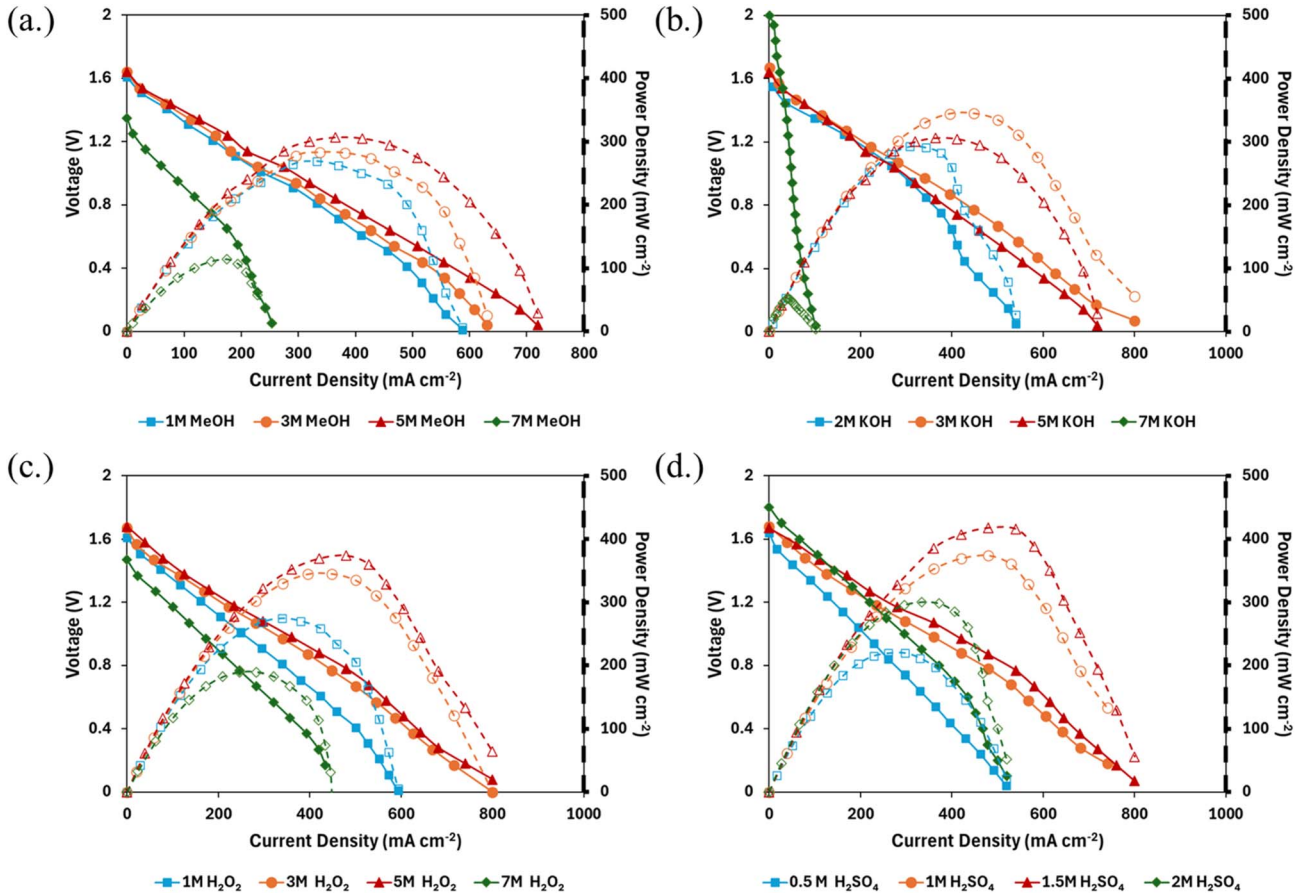

Fig. 3 Polarization and power density curve of the PMBI-DMHPFC with varying (a) MeOH concentration (KOH: 5 M, H_2O_2: 3 M, H_2SO_4: 1 M, membrane: N117, flow rate (anode and cathode): 1 ml min^{-1} cm^{-2}), (b) KOH concentration (MeOH: 5 M, H_2O_2: 3 M, H_2SO_4: 1 M, membrane: N117, flow rate (anode and cathode): 1 ml min^{-1} cm^{-2}), (c) H_2O_2 concentration (MeOH: 5 M, KOH: 3 M, H_2SO_4: 1 M, membrane: N117, flow rate (anode and cathode): 1 ml min^{-1} cm^{-2})and (d.) H_2SO_4 concentration (MeOH: 5 M, KOH: 3 M, H_2O_2: 5 M, membrane: N117, flow rate (anode and cathode): 1 ml min^{-1} cm^{-2}).

OCV from 1.61 V to 1.64 V and an increase in the PPD from 269 to 306 mW cm^{-2}. However, a further increase to 7 M proves detrimental. As depicted in Fig. 3a, at 7 M the OCV decreases significantly to 1.35 V, and the PPD decreases to 114 mW cm^{-2}. This decline suggests that methanol crossover is exacerbated at higher concentrations, leading to cathode catalyst poisoning. Beyond MeOH crossover, a higher methanol concentration also limits mass transport, leading to MeOH's excessive occupation of active sites. This, in turn, causes insufficient OH^- supply, greater OH^- concentration loss, and a decline in cell performance. Therefore, these findings demonstrate that 5 M MeOH provides the optimal balance between MOR kinetics, methanol crossover, and mass transport, leading subsequent experiments to prioritize a 5 M MeOH concentration to maximize power density.

The OH^- concentration also plays a pivotal role in determining the MOR kinetics at the anode. An adequate OH^- concentration is essential for facilitating the MOR, but excessively high concentrations can lead to electrode flooding, hinder mass transport, and cause greater ohmic overpotential. To investigate this effect, the PMBI-DMHPFC was evaluated with varying KOH concentrations (2 M, 3 M, 5 M, and 7 M) while maintaining a fixed MeOH concentration of 5 M (Fig. 3b). As shown in Fig. 3b, increasing the KOH concentration increased the OCV from 1.55 V to 2.0 V, which is attributed to the thermodynamic favorability of MOR at high OH^- concentrations.[19] Cell voltage increased with increasing KOH concentrations in the low current density region (<150 mA cm^{-2}). This is attributed to enhanced MOR kinetics due to increased OH^- concentration within the ACL and reduced activation overpotential. In contrast, at higher current densities, the optimal KOH concentration for cell performance was found to be 3 M. Higher KOH concentrations (5 M and 7 M) increased electrolyte viscosity, leading to high ohmic loss and limiting mass transport of reactants (MeOH) and product (CO_2). This is evidenced by the PPD, where the 3 M KOH showed the best results, balancing enhanced MOR kinetics with ohmic resistance and mass transport.

4.3 Effect of catholyte concentration

H_2O_2 concentration is a key parameter in PMBI-DMHPFCs, balancing enhanced HPRR kinetics with increased crossover,

decomposition, and mass transport limitations. The PMBI-DMHPFC was evaluated with H_2O_2 concentrations of 1 M, 3 M, 5 M, and 7 M, while maintaining a fixed 1 M sulfuric acid concentration (Fig. 3c). At low current densities, cell voltage increased with H_2O_2 concentration up to 5 M. However, at 7 M H_2O_2, increased diffusion across the membrane led to a mixed potential at the ACL, reducing OCV, indicating H_2O_2 crossover. At higher current densities, performance improved until 5 M H_2O_2. Raising the H_2O_2 concentration from 1 M to 5 M increased the PPD from 275 to 375 mW cm^{-2}, attributed to enhanced HPRR kinetics. A concentration of 7 M H_2O_2 reduced the PPD to 190 mW cm^{-2}. This is likely due to competition between H_2O_2 and H^+ for active sites on the catalyst and an increase in chemical decomposition at the cathode, which generates oxygen byproducts and limits mass transport. The polarization curve for 7 M H_2O_2 (Fig. 3c) exhibited a steeper voltage drop at higher current densities, consistent with increased mass transport limitations. Therefore, the subsequent experiments were run with a 5 M concentration as it offered the best compromise between enhanced kinetics and operational stability.

H_2SO_4 acts as a supporting electrolyte in the catholyte. In addition to improving solution conductivity, it facilitates H^+ transport to the electrode surface and reduces the charge transfer resistance, ultimately enhancing HPRR kinetics. The PMBI-DMHPFC was evaluated with H_2SO_4 concentrations of 0.5 M, 1 M, 1.5 M, and 2 M, maintaining a fixed 5 M H_2O_2 concentration (Fig. 3d). As shown in Fig. 3d, increasing the H_2SO_4 concentration increased the OCV from 1.64 V to 1.8 V, which is attributed to the thermodynamic favorability of HPRR at high H^+ concentrations. At low current densities, cell voltage increased with H_2SO_4 concentration, which is attributed to improved HPRR kinetics as protons in the CCL transition from deficiency to abundance, reducing cathode activation overpotential. However, at higher current densities, optimal cell performance was achieved with 1.5 M H_2SO_4. Although increasing the H_2SO_4 concentration slightly increased the internal resistance up to this point, it was outweighed by enhanced HPRR. The increased catholyte viscosity above this concentration hinders species migration leading to increased internal resistance. The slope of the polarization curve with 2 M H_2SO_4 was greater than with 1.5 M H_2SO_4, particularly after 200 mA cm^{-2}, demonstrating that increased internal resistance resulted in voltage drops(Fig. 3d). Furthermore, H^+ and H_2O_2 compete for active sites within the CCL. At 2 M sulfuric acid, excess H^+ occupy numerous active sites, reducing local H_2O_2 supply and HPRR kinetics, leading to significant concentration loss and deteriorating cell performance. The PMBI-DMHPFC with 1.5 M H_2SO_4 was found to perform best, having achieved the highest power density.

4.4 Effect of membrane thickness

The membrane thickness impacts PMBI-DMHPFC performance, affecting both species crossover rates and internal resistance. Thinner membranes decrease internal resistance, increase performance, and increase species crossover, creating mixed potentials and decreasing efficiency. Therefore, the PMBI-DMHPFC was evaluated with varying membrane thicknesses of NHP (20 μm), N212 (51 μm), N115 (127 μm) and N117 (183 μm) (Fig. 4a). The results presented in Fig. 4a suggest that the predominant factor affecting the cell performance varied with current density. Under low current density conditions, the mixed potential problem associated with the thinner membrane was found to be more serious, as evident in the decreasing OCV trend. NHP had the lowest OCV and PPD, suggesting significant crossover. At moderate and higher current densities, however, the effect of the internal resistance was found to become dominant. It should be mentioned that the rate of species crossover decreased with increasing current density, as higher current densities reduce the concentration gradient across the membrane and thus limit passive crossover. This contributes to the improved performance of N115 compared to N117 at higher current densities. It is worth mentioning that there are 2 species (MeOH and H_2O_2) in this system, resulting in the complicated species crossover phenomenon. The optimum balance between internal resistance and species crossover was observed for Nafion115. We acknowledge that the assignment of performance losses to internal resistance with varying membrane thickness is based on established trends for PEMs. However, comprehensive electrochemical impedance spectroscopy (EIS) studies are needed to confirm these observations quantitatively and will be incorporated in future work.

4.5 Effect of flow rate

The effect of flow rate ratio on PMBI-DMHPFC performance is illustrated in Fig. 4b, where the ratio of MeOH to H_2O_2 flow rates was varied (1 : 1, 1 : 3, and 3 : 1) with base flow rate to be 1 ml min^{-1} cm^{-2}. Asymmetric flow rates (1 : 3 and 3 : 1) significantly reduced OCV and PPD, indicating increased crossover effects and mass transport limitations. For instance, the lower PPD with the 1 : 3 ratio (low H_2O_2 residence time) indicates a H_2O_2-deficient cathode limiting the reaction rate. In contrast, the 3 : 1 ratio (low MeOH) suggests an MeOH-deficient anode hinders reaction kinetics. Furthermore, these asymmetric flow rates are expected to generate a pressure difference between the anode and cathode compartments. This pressure imbalance can place stress on the membrane, potentially exacerbating crossover and impacting long-term stability. In contrast, the balanced flow rate ratio 1 : 1 achieved optimal performance, with a high OCV and a PPD of approximately 460 mW cm^{-2}. The high OCV observed with this ratio minimizes methanol and H_2O_2 crossover by ensuring an adequate and balanced supply of both reactants to their respective electrodes, preventing excessive accumulation or depletion. In conclusion, maintaining a 1 : 1 flow rate ratio is essential for maximizing PMBI-DMHPFC performance by balancing reactant supply, minimizing crossover, and ensuring stable operation.

Fig. 4c shows the polarization curves with different flow rates in the cell. The motivation for increasing the flow rate was to remove CO_2 and O_2 bubbles from the anode and cathode electrodes. CO_2 and O_2 bubbles can increase mass transport losses,

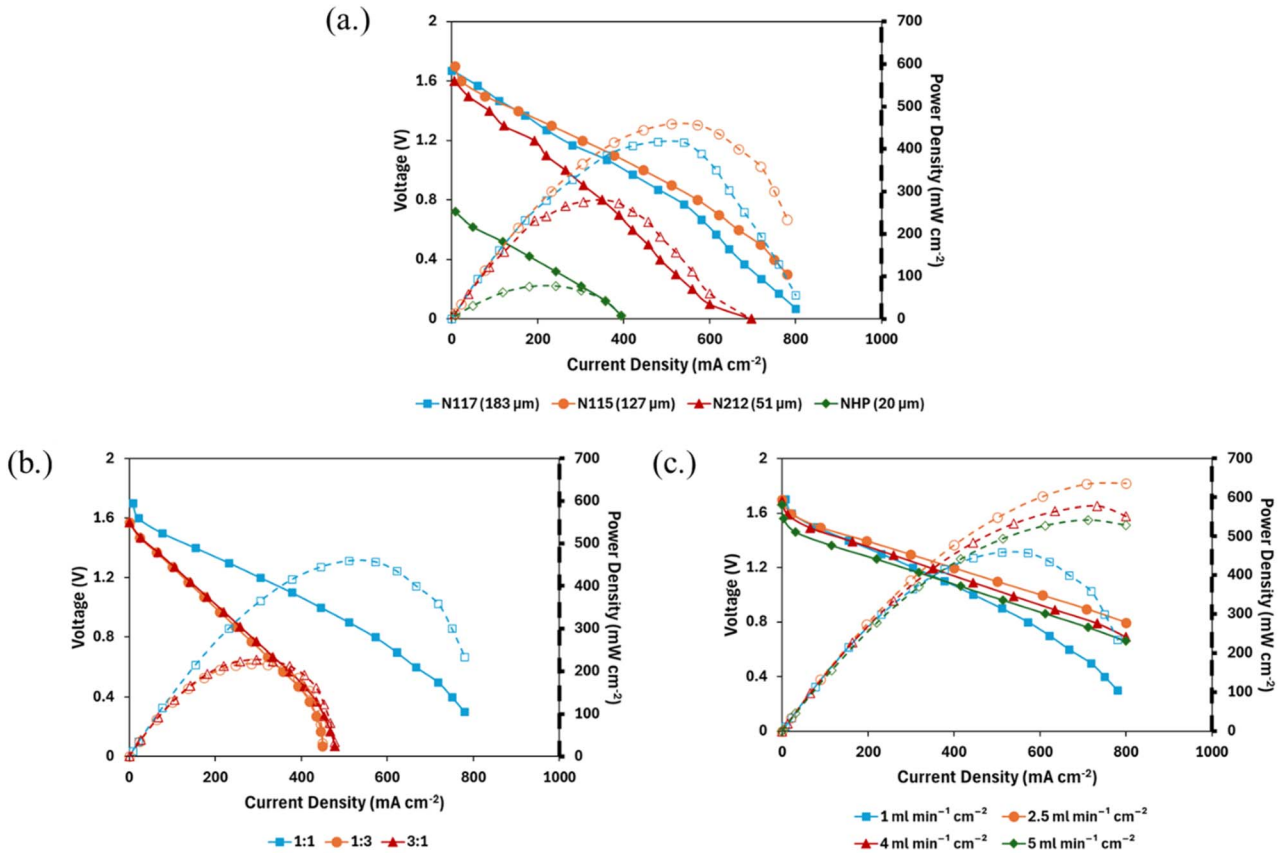

Fig. 4 Polarization and power density curve of the PMBI-DMHPFC with varying (a) membrane thickness (MeOH: 5 M, KOH: 3 M, H_2O_2: 5 M, H_2SO_4: 1.5 M, flow rate (anode and cathode): 1 ml min^{-1} cm^{-2}), (b) flow rate ratio (MeOH: 5 M, KOH: 3 M, H_2O_2: 5 M, H_2SO_4: 1.5 M, membrane: N115, base flow rate: 1 ml min^{-1} cm^{-2}), (c.) flow rate (MeOH: 5 M, KOH: 3 M, H_2O_2: 5 M, H_2SO_4: 1.5 M, membrane: N115).

as the bubbles can block the reactant flow and hinder the transport of reactants to the reaction sites. Excessive CO_2 and O_2 accumulation and bubble formation can also damage the PEM, reducing the PMBI-DMHPFC's performance and lifetime. At the cathode, key considerations include limiting the contact duration between the catalyst and the electrolyte to minimize H_2O_2 decomposition, improving reactant utilization by increasing contact duration, and removing O_2 gas bubbles from the catalyst surface to improve HPRR. Hence, increasing electrolyte velocity to remove the adhering bubbles is desirable, but very high velocity will limit the contact time for MOR and HPRR. At high current densities, the 1 ml min^{-1} cm^{-2} flow rate's polarization curve exhibited steep voltage drops, indicating significant mass transport limitations due to CO_2 and O_2 bubble accumulation. CO_2 and O_2 bubbles detach from the electrodes as the flow rate increases. However, beyond 2.5 ml min^{-1} cm^{-2}, the contact duration was limited, hindering both MOR and HPRR. The balance between removing CO_2 and O_2 bubbles and contact duration for reactant utilization led to the optimum flow rate of 2.5 ml min^{-1} cm^{-2}.

4.6 Constant-current discharge behavior

A constant current discharge test was performed to verify the PMBI-DMHPFC's stability and durability at the identified optimal operational conditions. A fuel solution containing 5.0 M MeOH and 3.0 M KOH and an oxidant solution containing 5 M hydrogen peroxide and 1.5 M sulfuric acid were fed into the cell at a flow rate of 2.5 ml min^{-1} cm^{-2}. The operating temperature was 80 °C, and the discharge current density was

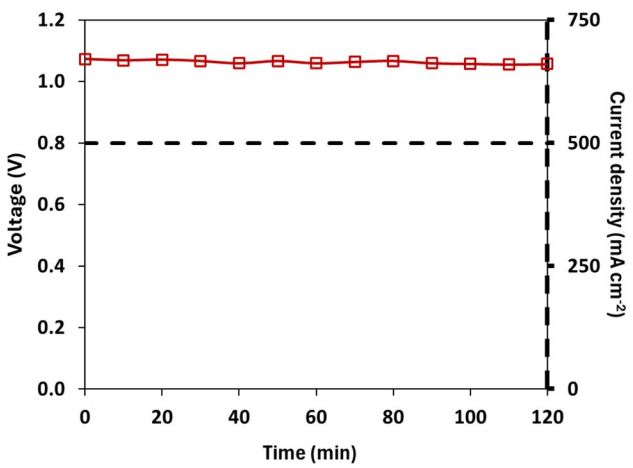

Fig. 5 Constant-current discharging behavior of PMBI-DMHPFC at a current density of 500 mA cm^{-2} (MeOH: 5 M, KOH: 3 M, H_2O_2: 5 M, H_2SO_4: 1.5 M, membrane: N115, flow rate: 2.5 ml min^{-1} cm^{-2}).

500 mA cm^{-2}. Fig. 5 shows the constant current discharge behavior, demonstrating stable cell operation for 2 hours and proving the feasibility of this PMBI-DMHPFC configuration. The present study demonstrates a 2-hour stable operation. However, to establish the DMHPFC's long-term viability, extended (>24 h) constant current discharge tests are warranted. Factors affecting fuel cell life likely include catalyst poisoning, membrane degradation, and H_2O_2 decomposition. Ongoing studies will address these durability challenges quantitatively.

5 Conclusion

A DMHPFC with a PMBI configuration was developed by employing a highly conductive AEI as the anode binder and Nafion as the membrane separator and leveraging an alkaline anode and acidic cathode. This PMBI-DMHPFC demonstrated significantly improved performance compared to conventional DMFCs using O_2 and H_2O_2 as oxidants. The performance of the PMBI-DMHPFC was evaluated under various conditions, including anolyte and catholyte concentrations, membrane thickness, and flow rate. The cell achieved a current density of 500 mA cm^{-2} at 1.1 V and a peak power density (PPD) of 630 mW cm^{-2} at 0.8 V. A high open circuit voltage (OCV) of 1.69 V was observed, which was attributed to the effective local separation of anolyte and catholyte at the electrocatalytically active sites. A 2-hour constant current discharge curve demonstrated stable operation, further validating the PMBI-DMHPFC's reliability. Despite these advancements, certain aspects remain unexplored. For instance, overpotentials associated with the HPRR at the cathode require further investigation. Reducing cathode overpotentials could enable this type of PMBI-DMHPFC to power propulsion systems for autonomous vehicles. Additionally, MeOH and H_2O_2 crossover effects must be studied with alternative PEMs beyond Nafion, as this has the potential to reduce ohmic overpotentials further. Future research on advanced electrocatalysts and optimized membrane materials has the potential to enhance performance further and broaden the applicability of this technology. This work also highlights opportunities to extend the PMBI-enabled approach to other liquid fuels, such as ethanol, propanol, and glycerol, which exhibit lower oxidation potential in alkaline media. By leveraging H_2O_2 as an oxidant, significant performance improvements can be achieved in these systems. Furthermore, hybrid battery-fuel-cell systems, with batteries and a supercapacitor for peak power and the fuel cell for base load, offer a solution and improve PMBI-DMHPFCs' potential as an H_2-PEMFC alternative.

Conflicts of interest

The authors declare that they have no known competing financial interests or personal relationships that could have appeared to influence the work reported in this paper. Some of the authors are named inventors on US patents 11,949,136 and 11,616,246 which are related to the technologies described in this work and these patents have been assigned to Washington University in St. Louis.

Data availability

Supplementary information: The data supporting this article have been included as part of the SI. See DOI: **https://doi.org/10.1039/d5se01042j**.

Acknowledgements

This project has received funding from ONR, N00014-16-1-2833. SS gratefully acknowledges support from the University of Texas at San Antonio. ZW gratefully acknowledges support from the University of Alabama, Tuscaloosa, through a startup grant.

References

1 N. A. A. Qasem and G. A. Q. Abdulrahman, A Recent Comprehensive Review of Fuel Cells: History, Types, and Applications, *Int. J. Energy Res.*, 2024, **2024**, 7271748, DOI: **10.1155/2024/7271748**.
2 M. Yang, R. Hunger, S. Berrettoni, B. Sprecher and B. Wang, A review of hydrogen storage and transport technologies, *Clean Energy*, 2023, **7**, 190–216, DOI: **10.1093/CE/ZKAD021**.
3 M. T. Ahad, M. M. H. Bhuiyan, A. N. Sakib, A. Becerril Corral and Z. Siddique, An Overview of Challenges for the Future of Hydrogen, *Materials*, 2023, **16**, 6680, DOI: **10.3390/MA16206680**.
4 M. Nacef and A. M. Affoune, Comparison between direct small molecular weight alcohols fuel cells' and hydrogen fuel cell's parameters at low and high temperature. Thermodynamic study, *Int. J. Hydrogen Energy*, 2011, **36**, 4208–4219, DOI: **10.1016/j.ijhydene.2010.06.075**.
5 H. Ahmad, S. K. Kamarudin, U. A. Hasran and W. R. W. Daud, Overview of hybrid membranes for direct-methanol fuel-cell applications, *Int. J. Hydrogen Energy*, 2010, **35**, 2160–2175, DOI: **10.1016/j.ijhydene.2009.12.054**.
6 S. Basri, S. K. Kamarudin, W. R. W. Daud and Z. Yaakub, Nanocatalyst for direct methanol fuel cell (DMFC), *Int. J. Hydrogen Energy*, 2010, **35**, 7957–7970, DOI: **10.1016/j.ijhydene.2010.05.111**.
7 C. Zhao, H. Lin and H. Na, Novel cross-linked sulfonated poly (arylene ether ketone) membranes for direct methanol fuel cell, *Int. J. Hydrogen Energy*, 2010, **35**, 2176–2182, DOI: **10.1016/j.ijhydene.2009.12.149**.
8 *Methanol – Global Strategic Business Report*, **https://www.researchandmarkets.com/reports/338607/methanol_global_strategic_business_report?utm_source=GNE&utm_medium=PressRelease&utm_code=jj7v7p&utm_campaign=2034987+-+Methanol+Global+Forecast+Report+2025-2030%2c+with+Profiles+of+100%2b+Key+Players+including+BASF%2c+Equinor%2c+HELM%2c+Methanex%2c+Mitsui%2c+Repsol%2c+Sipchem+and+More&utm_exec=carimspi**, accessed June 10, 2025.
9 *Methanol Price Trends & Forecast, Monthly, Quarterly, Yearly Data (2024-2025)*, **https://nexizo.ai/blogs/methanol-price-trends-forecast**, accessed June 10, 2025.

10 B. L. Garc'ia and J. W. Weidner, Review of Direct Methanol, *Fuel Cells*, 2007, 229–284, DOI: 10.1007/978-0-387-46106-9_5.
11 S. S. Araya, V. Liso, X. Cui, N. Li, J. Zhu, S. L. Sahlin, S. H. Jensen, M. P. Nielsen and S. K. Kær, A Review of The Methanol Economy: The Fuel Cell Route, *Energies*, 2020, **13**, 596, DOI: 10.3390/EN13030596.
12 C. Lamy, A. Lima, V. LeRhun, F. Delime, C. Coutanceau and J. M. Léger, Recent advances in the development of direct alcohol fuel cells (DAFC), *J. Power Sources*, 2002, **105**, 283–296, DOI: 10.1016/S0378-7753(01)00954-5.
13 A. S. Aricò, S. Srinivasan and V. Antonucci, DMFCs: From Fundamental Aspects to Technology Development, *Fuel Cells*, 2001, **1**, 133–161, DOI: 10.1002/1615-6854(200107)1:2<133::aid-fuce133>3.3.co;2-x.
14 S. Sui, X. Wang, X. Zhou, Y. Su, S. Riffat and C. jun Liu, A comprehensive review of Pt electrocatalysts for the oxygen reduction reaction: Nanostructure, activity, mechanism and carbon support in PEM fuel cells, *J. Mater. Chem. A*, 2017, **5**, 1808–1825, DOI: 10.1039/C6TA08580F.
15 L. An, T. Zhao, X. Yan, X. Zhou and P. Tan, The dual role of hydrogen peroxide in fuel cells, *Sci. Bull.*, 2015, **60**, 55–64, DOI: 10.1007/s11434-014-0694-7.
16 R. K. Raman and A. K. Shukla, Electro-reduction of hydrogen peroxide on iron tetramethoxy phenyl porphyrin and lead sulfate electrodes with application in direct borohydride fuel cells, *J. Appl. Electrochem.*, 2005, **35**, 1157–1161, DOI: 10.1007/s10800-005-9021-y.
17 R. K. Raman and A. K. Shukla, A direct borohydride/hydrogen peroxide fuel cell with reduced alkali crossover, *Fuel Cells*, 2007, **7**, 225–231, DOI: 10.1002/fuce.200600023.
18 *Bond Enthalpies*, https://owl.oit.umass.edu/departments/Chemistry/appendix/bond.html, accessed July 1, 2024.
19 E. H. Yu, K. Scott, R. W. Reeve, L. Yang and R. G. Allen, Characterisation of platinised Ti mesh electrodes using electrochemical methods: Methanol oxidation in sodium hydroxide solutions, *Electrochim. Acta*, 2004, **49**, 2443–2452, DOI: 10.1016/j.electacta.2004.01.022.
20 A. I. Dalton and J. V Bauer, *Method of stabilizing hydrogen peroxide solutions*, 1980.
21 M. Pourbaix, *Atlas of Electrochemical Equilibria In-Aqueous Solutions*, 1974.
22 M. Ünlü, J. Zhou and P. A. Kohl, Hybrid anion and proton exchange membrane fuel cells, *J. Phys. Chem. C*, 2009, **113**, 11416–11423, DOI: 10.1021/JP903252U/ASSET/IMAGES/LARGE/JP-2009-03252U_0008.JPEG.
23 J. Chen, K. Sharma, Z. Wang, S. Sankarasubramanian and V. Ramani, Microscale Bipolar Interfaces for High-Power Fuel Cells, *Acc. Mater. Res.*, 2025, **6**(7), 865–875, DOI: 10.1021/ACCOUNTSMR.5C00039/ASSET/IMAGES/LARGE/MR5C00039_0007.JPEG.
24 Z. Wang, J. Parrondo, C. He, S. Sankarasubramanian and V. Ramani, Efficient pH-gradient-enabled microscale bipolar interfaces in direct borohydride fuel cells, *Nat. Energy*, 2019, **4**, 281–289, DOI: 10.1038/s41560-019-0330-5.
25 Z. Wang, M. Mandal, S. Sankarasubramanian, G. Huang, P. A. Kohl and V. K. Ramani, Influence of Water Transport Across Microscale Bipolar Interfaces on the Performance of Direct Borohydride Fuel Cells, *ACS Appl. Energy Mater.*, 2020, **3**(5), 4449–4456, DOI: 10.1021/acsaem.0c00145.
26 Z. Wang, S. Sankarasubramanian and V. Ramani, Reactant-Transport Engineering Approach to High-Power Direct Borohydride Fuel Cells, *Cell Rep. Phys. Sci.*, 2020, **1**, 100084, DOI: 10.1016/J.XCRP.2020.100084.
27 D. N. Prater and J. J. Rusek, Energy density of a methanol/hydrogen-peroxide fuel cell, *Appl. Energy*, 2003, **74**, 135–140, DOI: 10.1016/S0306-2619(02)00139-3.
28 A. Uddin, L. Dunsmore, H. Zhang, L. Hu, G. Wu and S. Litster, High Power Density Platinum Group Metal-free Cathodes for Polymer Electrolyte Fuel Cells, *ACS Appl. Mater. Interfaces*, 2020, **12**, 2216–2224, DOI: 10.1021/ACSAMI.9B13945/ASSET/IMAGES/LARGE/AM9B13945_0008.JPEG.
29 L. Osmieri, R. Escudero-Cid, A. H. A. Monteverde Videla, P. Ocón and S. Specchia, Performance of a Fe-N-C catalyst for the oxygen reduction reaction in direct methanol fuel cell: Cathode formulation optimization and short-term durability, *Appl. Catal., B*, 2017, **201**, 253–265, DOI: 10.1016/j.apcatb.2016.08.043.
30 R. Bashyam and P. Zelenay, A class of non-precious metal composite catalysts for fuel cells, *Nature*, 2006, **443**, 63–66, DOI: 10.1038/nature05118.
31 G. T. K. K. Gunasooriya and M. Saeys, CO Adsorption on Pt(111): From Isolated Molecules to Ordered High-Coverage Structures, *ACS Catal.*, 2018, **8**, 10225–10233, DOI: 10.1021/ACSCATAL.8B02371/ASSET/IMAGES/LARGE/CS-2018-02371B_0006.JPEG.
32 C. Molochas and P. Tsiakaras, Carbon Monoxide Tolerant Pt-Based Electrocatalysts for H2-PEMFC Applications: Current Progress and Challenges, *Catalysts*, 2021, **11**, 1127, DOI: 10.3390/CATAL11091127.
33 A. H. Ali and P. G. Pickup, Electrolysis of Ethanol and Methanol at PtRu@Pt Catalysts, *J. Electrochem. Soc.*, 2022, **169**, 034523.
34 M. T. Darby, E. C. H. Sykes, A. Michaelides and M. Stamatakis, Carbon Monoxide Poisoning Resistance and Structural Stability of Single Atom Alloys, *Top. Catal.*, 2018, **61**, 428–438, DOI: 10.1007/S11244-017-0882-1/FIGURES/8.
35 S. Y. Huang and C. T. Yeh, Promotion of the electrocatalytic activity of a bimetallic platinum-ruthenium catalyst by repetitive redox treatments for direct methanol fuel cell, *J. Power Sources*, 2010, **195**, 2638–2643, DOI: 10.1016/j.jpowsour.2009.11.049.
36 O. Sahin and H. Kivrak, A comparative study of electrochemical methods on Pt-Ru DMFC anode catalysts: The effect of Ru addition, *Int. J. Hydrogen Energy*, 2013, **38**, 901–909, DOI: 10.1016/j.ijhydene.2012.10.066.
37 A. Kormanyos, P. Büttner, M. Bosch, M. Minichova, A. Körner, K. J. Jenewein, A. Hutzler, K. J. J. Mayrhofer, J. Bachmann and S. Cherevko, Stability of Bimetallic PtxRuy – From Model Surfaces to Nanoparticulate Electrocatalysts, *ACS Mater. Au*, 2024, **4**, 286–299, DOI: 10.1021/ACSMATERIALSAU.3C00092/ASSET/IMAGES/LARGE/MG3C00092_0006.JPEG.

38 S. C. Zignani, V. Baglio, D. Sebastián, T. A. Rocha, E. R. Gonzalez and A. S. Aricò, Investigation of PtNi/C as methanol tolerant electrocatalyst for the oxygen reduction reaction, *J. Electroanal. Chem.*, 2016, **763**, 10–17, DOI: 10.1016/J.JELECHEM.2015.12.044.

39 T. Ioroi, K. Yasuda, Z. Siroma, N. Fujiwara and Y. Miyazaki, Enhanced CO-Tolerance of Carbon-Supported Platinum and Molybdenum Oxide Anode Catalyst, *J. Electrochem. Soc.*, 2003, **150**, A1225, DOI: 10.1149/1.1598211/XML.

40 Y. W. Zhou, Y. F. Chen, K. Jiang, Z. Liu, Z. J. Mao, W. Y. Zhang, W. F. Lin and W. Bin Cai, Probing the enhanced methanol electrooxidation mechanism on platinum-metal oxide catalyst, *Appl. Catal., B*, 2021, **280**, 119393, DOI: 10.1016/j.apcatb.2020.119393.

41 E. H. Yu, K. Scott, R. W. Reeve, L. Yang and R. G. Allen, Characterisation of platinised Ti mesh electrodes using electrochemical methods: Methanol oxidation in sodium hydroxide solutions, *Electrochim. Acta*, 2004, **49**, 2443–2452, DOI: 10.1016/j.electacta.2004.01.022.

42 R. Serra-Maia, M. Bellier, S. Chastka, K. Tranhuu, A. Subowo, J. D. Rimstidt, P. M. Usov, A. J. Morris and F. M. Michel, Mechanism and Kinetics of Hydrogen Peroxide Decomposition on Platinum Nanocatalysts, *ACS Appl. Mater. Interfaces*, 2018, **10**, 21224–21234, DOI: 10.1021/ACSAMI.8B02345/ASSET/IMAGES/MEDIUM/AM-2018-02345R_M017.GIF.

43 F. F. Liu and C.-Y. Wang, Mixed Potential in a Direct Methanol Fuel Cell Modeling and Experiments, *J. Electrochem. Soc.*, 2007, **154**, B514.

44 X. H. Yan, T. S. Zhao, L. An, G. Zhao and L. Zeng, A novel cathode architecture with a thin reaction layer alleviates mixed potentials and catalyst poisoning in direct methanol fuel cells, *Int. J. Hydrogen Energy*, 2015, **40**, 16540–16546, DOI: 10.1016/j.ijhydene.2015.10.039.

45 Z. Wang, J. Parrondo and V. Ramani, Anion Exchange Membranes Based on Polystyrene- Block -Poly(ethylene-ran -butylene)- Block -Polystyrene Triblock Copolymers: Cation Stability and Fuel Cell Performance, *J. Electrochem. Soc.*, 2017, **164**, F1216–F1225, DOI: 10.1149/2.1561712JES/XML.